Atmos. Chem. Phys. Discuss., 13, 11315–11355, 2013
www.atmos-chem-phys-discuss.net/13/11315/2013/
doi:10.5194/acpd-13-11315-2013


Atmospheric Chemistry and Physics Discussions



# The impact of emissions and climate change on ozone in the United States under Representative Concentration Pathways (RCPs)

**Y. Gao[1], J. S. Fu[1], J. B. Drake[1], J.-F. Lamarque[2], and Y. Liu[3]**

[1]Department of Civil and Environmental Engineering, University of Tennessee, Knoxville, Tennessee, USA
[2]Atmospheric Chemistry and Climate and Global Dynamics Divisions, National Center for Atmospheric Research, Boulder, Colorado, USA
[3]Rollins School of Public Health, Emory University, Atlanta, Georgia, USA

Received: 20 February 2013 – Accepted: 18 April 2013 – Published: 26 April 2013

Correspondence to: J. S. Fu (jsfu@utk.edu)

Published by Copernicus Publications on behalf of the European Geosciences Union.







## Abstract

Dynamical downscaling was applied in this study to link the global climate–chemistry model Community Atmosphere Model (CAM-Chem) with the regional models: Weather Research and Forecasting (WRF) Model and Community Multi-scale Air Quality (CMAQ). Two Representative Concentration Pathway (RCP) scenarios (RCP 4.5 and RCP 8.5) were used to evaluate the climate impact on ozone concentrations in 2050s.

Ozone concentrations in the lower-mid troposphere (surface to ~ 300 hPa), from mid- to high latitudes in the Northern Hemisphere (NH), show decreasing trends in RCP 4.5 between 2000s and 2050s, with the largest decrease of 4–10 ppbv occurring in the summer and the fall; and increasing trends (2–12 ppbv) in RCP 8.5 resulting from the increased methane emissions. In RCP 8.5, methane emissions increase by ~ 60 % by the end of 2050s, accounting for more than 90 % of ozone increases in summer and fall, and 60–80 % in spring and winter.

Under the RCP 4.5 scenario, in the summer when photochemical reactions are the most active, the large ozone precursor emissions reduction leads to the greatest decrease of downscaled surface ozone concentrations, ranging from 6 to 10 ppbv. However, a few major cities show ozone increases of 3 to 7 ppbv due to weakened NO titration. Under the RCP 8.5 scenario, in winter, downscaled ozone concentrations increase across nearly the entire continental US in winter, ranging from 3 to 10 ppbv due to increased methane emissions and enhanced stratosphere-troposphere exchange (STE). More intense heat waves are projected to occur by the end of 2050s in RCP 8.5, leading to more than 8 ppbv of the maximum daily 8 h daily average (MDA8) ozone during the heat wave days than other days; this indicates the dramatic impact heat waves exert on high frequency ozone events.





ACPD

13, 11315–11355, 2013



## 1 Introduction

The Special Report on Emissions Scenarios (SRES; Nakicenovic and Swart, 2000) have been designed and the Coupled Model Intercomparison Project phase 3 (CMIP3) simulations have been conducted in support of the Intergovernmental Panel on Climate Change (IPCC) Fourth Assessment Report (Solomon et al., 2007). As a result, climate change under the SRES scenarios has been fully evaluated (Annan and Hargreaves, 2011; Meehl et al., 2005, 2007). Likewise, "representative concentration pathways[1]" (RCPs, Moss et al., 2010) scenarios were designed and the CMIP Phase 5 (CMIP5) (Taylor et al., 2009, 2012) simulations were conducted to investigate the impact of greenhouse gases on climate change for the upcoming IPCC Fifth Assessment Report (AR5).

Recent comparisons and evaluations of climate between CMIP3 and CMIP5 models (Stroeve et al., 2012; Knutti and Sedlacek, 2013; Rogelj et al., 2012; Judah et al., 2012) have shown that climate change strongly impacts regional meteorology and air quality. Thus, researchers have performed sensitivity studies to investigate the effects of perturbations in climate on air quality, and these studies were recently reviewed and discussed by Jacob and Winner (2009) and Fiore et al. (2012). In order to further evaluate the relationships between atmospheric chemistry and climate change, and to support the IPCC AR5, the Atmospheric Chemistry and Climate Model Intercomparison Project (ACCMIP) (Lamarque et al., 2012b) has been established to explore the impact of climate under the RCP scenarios on global atmospheric chemistry and air quality with spatial resolutions of 1–2 degrees or coarser. Global chemistry models predict that by the end of 21st century, tropospheric ozone will decrease under the RCP 2.6, RCP 4.5 and RCP 6.0 scenarios, and increase under the RCP 8.5 scenario (Lamarque et al., 2011a; Kawase et al., 2011; Young et al., 2012).

However, due to the coarse spatial resolutions, global studies often lack useful local air quality information, which could be applied to policy strategies. Thus, a technique,

[1] http://www.iiasa.ac.at/web-apps/tnt/RcpDb/dsd?Action=htmlpage&page=about





ACPD
13, 11315–11355, 2013



called dynamical downscaling (Caldwell et al., 2009; Lam and Fu, 2009), is commonly used to link global and regional models. This is done by applying the initial and boundary conditions from global models to serve as drivers of regional models and results in high resolution simulations. Dynamical downscaling has been widely used in evaluating regional air quality under the IPCC SRES scenarios.

Bell et al. (2007) found that under the IPCC SRES A2 climate scenario (spatial resolution of 36 km, emissions kept at present levels), summer hourly ozone across 50 cities in the eastern US was projected to increase by an average of 4.8 ppbv with a maximum of 9.6 ppbv by the 2050s. They also found that the mean number of days exceeding the maximum daily 8 h ozone (MDA8) regulatory standard increased by 68 %. While maintaining emissions at current levels and using a spatial resolution of 36 km, Nolte et al. (2008) found, an overall increase from 2 to 5 ppbv in MDA8 in Texas and parts of the eastern US under A1B scenario by the 2050s. By using a global chemistry model (Model for OZone And Related Chemical Tracers, MOZART) with a spatial resolution of 30 km, Huang et al. (2008) found that the five-summer mean ozone concentrations increase by 4 % to 9 % in most US regions in the 2050s with increased anthropogenic emissions under the A1FI scenario. In the eastern US, Lam et al. (2011) found 2 to 5 ppbv increase of MDA8 with climate change under A1B scenario; a ∼5 ppbv decrease from the combined effect of climate change and emission reductions was found with spatial resolutions of 36/12 km. It is worth noting that these different scenarios have different levels of ozone precursor emissions, including methane.

Until now, there were very limited applications of dynamical downscaling under the new RCP scenarios. Kelly et al. (2012) used a Unified Regional Air-quality Modelling System (AURAMS) on a 45 km × 45 km resolution grid and found, under A2 climate and RCP 6.0 ozone precursor emissions, that ozone concentrations decrease for most of the US. The mixture of SRES climate and RCP emissions makes it difficult to classify this study as either an SRES or RCP scenario.

Another important issue is spatial resolution. High resolution (12 km) could produce a better representation of atmospheric circulation and topographic features, while





ACPD
13, 11315–11355, 2013



36 km is too coarse to resolve important regional details, particularly in mountainous areas (Mass et al., 2002; Caldwell et al., 2009). All these studies, including both SRES and RCPs, have spatial resolutions of 30 km or coarser (except Lam et al., 2011 applies 12 km in eastern US), which may not be able to well capture topography and climate details.

Under both SRES (Ganguly et al., 2009; Meehl and Tebaldi, 2004) and RCP (Gao et al., 2012; Meehl et al., 2011) scenarios, more intense heat waves were projected to occur in future climate conditions. Heat waves have been reported to increase ozone concentrations dramatically. During the first two weeks of August 2003, heat waves in the UK cause mean population-weighted ozone concentration to reach as high as 103 $\mu g\,m^{-3}$, while ozone concentrations were only around 58 $\mu g\,m^{-3}$ during the same period in 2002 (Stedman, 2004). During the heat waves in 2003, Vieno et al. (2010) found that a temperature increase of 5 °C could lead to a surface ozone increase of up to 9 ppbv at Writtle (70 km northeast of London). Although heat waves have been widely investigated under future climate scenarios (Ganguly et al., 2009; Meehl and Tebaldi, 2004; Gao et al., 2012; Meehl et al., 2011), their impact on ozone concentrations have not attracted the same amount of attention under the same climate scenarios.

Thus, to provide more reasonable high-resolution information, this study is the first assessment to apply the dynamical downscaling technique under the new RCP scenarios with a spatial resolution of 12 km by 12 km over the continental US region. This paper documents the downscaling methodology, investigates the tropospheric ozone changes under future climate conditions, and evaluates the impact of heat waves on ozone concentrations in US.

## 2 Model description and configuration

Dynamical downscaling involves both global and regional climate–chemistry models. In this study, global climate model Community Earth System Model (CESM) version 1.0 was used to conduct global climate simulations. There are four major components





ACPD
13, 11315–11355, 2013



in CESM: Community Atmosphere Model(CAM4) (Neale et al., 2010), Community Land Model (CLM4) (Oleson, 2010), Parallel Ocean Program version 2 (POP2) (Smith, 2010), and Los Alamos National Laboratory Sea Ice Model, version 4 (CICE4) (Hunke and Lipscomb, 2008). The CESM was run with a spatial resolution of 0.9 (latitude) by 1.25 (longitude) degrees and 26 vertical layers with model top at ∼3 hPa (Neale et al., 2010). The atmospheric chemistry integrated in the atmosphere component CAM4 in CESM is referred to as CAM-Chem and is discussed in detail by Lamarque et al. (2012a). CAM-Chem has been widely used and evaluated on its representation in the atmosphere (Aghedo et al., 2011; Lamarque et al., 2012a, 2011a, b; Lamarque and Solomon, 2010). The atmospheric chemistry is computed at the same resolution (horizontal and vertical) as the atmosphere model. In order for the performed simulations to be consistent with the simulations performed for CMIP5 (without chemistry; Meehl et al., 2012), the simulated chemical fields do not affect the simulated climate, eliminating the risk of generating a different climate than the original CESM simulations. For the downscaling, three-hourly outputs were archived to provide initial and boundary conditions for the regional chemistry model.

Regional climate model WRF 3.2.1 (Skamarock and Klemp, 2008) was used in the regional climate simulations. The configurations of WRF have been discussed by Gao et al. (2012), and the major physics options include the Single-Moment 6-class microphysical scheme (WSM6) (Hong and Lim, 2006), the new Kain–Fritsch convective parameterization (Kain, 2004), the Rapid Radiative Transfer Model for Global Climate Models (GCMs) (RRTMG) longwave and shortwave radiation (Iacono et al., 2008; Morcrette et al., 2008), the Mellor–Yamada–Janjic planetary boundary layer (PBL) scheme (Janjić, 1990; Mellor and Yamada, 1982), and the Noah land surface model (Chen and Dudhia, 2001). There are a total of 34 vertical layers with model top pressure at 50 hPa.

The latest version of regional chemistry model Community Multi-scale Air Quality (CMAQ) modeling system version 5.0 (Wong et al., 2012) was used for the regional air quality simulations. Since its first release in 1998, tremendous efforts have been made by the United States Environmental Protection Agency (US EPA) (Wong et al.,





ACPD
13, 11315–11355, 2013



2012; Byun and Schere, 2006) and air quality modeling community to develop and improve the model. The CMAQ model has become a three dimensional comprehensive atmospheric chemistry and transport model, and has been widely used in air quality modeling community (Fu et al., 2012a, b; Huang et al., 2012; Wong et al., 2012; Nolte et al., 2008). The same model top pressure as WRF (50 hPa), and 14 vertical layers were applied to take into account computational limitations. WRF outputs were processed by the Meteorology-Chemistry Interface Processor (MCIP) (Otte and Pleim, 2010) in order to be used as CMAQ inputs.

Figure 1 shows the regional WRF-CMAQ simulation domain with a spatial resolution of 12 km by 12 km, and covers parts of Canada, Mexico, and the continental US. According to the National Climatic Data Center (NCDC)[2], the continental US can be divided into nine climate regions, which are the major focus areas in this study.

In addition to present climate (1850–2005), a total of four RCP scenarios (2005–2100), including RCP 2.6, RCP 4.5, RCP 6.0 and RCP 8.5, have been designed for the CMIP5. Due to limited computational resources, RCP 4.5 and RCP 8.5 were selected for this study. The central purposes of the selection were to evaluate and compare the climate and air quality under a low-to-medium emission scenario (RCP 4.5, Smith and Wigley, 2006; Wise et al., 2009) and a fossil fuel intensive emission scenario (RCP 8.5, Riahi et al., 2007). CAM-Chem was used to conduct global simulations from 2001 to the end of the 21st century continuously. The comparison with observations of CAM-Chem has been fully documented by Lamarque et al. (2012a) and its application to the RCP simulations is discussed in Lamarque et al. (2011a). After the global chemistry simulations, considering the computational limitations, a four-year period (2001–2004) and three-year period (2057–2059) were used to evaluate the impact of present climate and future climate on air quality. The selection of the present climate (2001–2004) considers the closest climate period before the start year (2005) of the RCP scenarios, while future climate in 2050s potentially captures enough climate change.

[2]http://www.ncdc.noaa.gov/temp-and-precip/us-climate-regions.php





ACPD
13, 11315–11355, 2013



## 3 Dynamical downscaling

Dynamical downscaling is a technique that uses the outputs from global climate or chemistry models to provide the initial and boundary conditions for the regional models. The downscaling process involves species mapping; and horizontal and vertical interpolations.

### 3.1 Species mapping from CAM-Chem to CMAQ

The first step for downscaling is to map the species in the global chemistry model CAM-Chem to the regional chemistry model CMAQ, listed in Table 1 (Emmons et al., 2010; Yarwood et al., 2005). During this process, most species can be mapped directly between these two models, except secondary organic aerosols (SOA). A bulk aerosol model was used in CAM-Chem (Lamarque et al., 2012a); thus, only combined anthropogenic and biogenic SOA was generated. However, a more sophisticated aerosol scheme (AE6) was implemented in CMAQ 5.0 and includes 24 semi-volatile SOA and 7 nonvolatile SOA (Carlton et al., 2010). No universal ratios can be used to partition the combined anthropogenic and biogenic SOA to different SOA species. As suggested by Carlton et al. (2010), CMAQ simulations driven by the default profile initial and boundary conditions were conducted. Then the ratios among the SOA species were used to allocate each SOA species based on the combined SOA.

### 3.2 Initial and boundary conditions

For the downscaling process, CAM-Chem was used to provide the initial and boundary conditions for CMAQ. Initial conditions are needed only for the first time step while three hourly boundary conditions were generated to achieve better diurnal representation.

It is important to keep the downscaled initial and boundary conditions consistent with the CAM-Chem outputs. Figure 2 shows the surface boundary conditions for the continental US domain used in CMAQ and the corresponding grids in CAM-Chem on





ACPD
13, 11315–11355, 2013



1 July 2001, for example. Due to the differences of spatial resolutions between CAM-Chem and CMAQ, the grid cells in CAM-Chem closest to the CMAQ domain were used. A comparison of the models, Fig. 2a and b, shows that they are consistent with each other along the four boundaries. Other variables and the initial conditions have also been checked and consistent patterns were found (not shown here).

### 3.3 Emission inventory and emission factor projections

The emission projections in other areas of the world show different patterns (Fig. 3). In both the RCP 4.5 and RCP 8.5 scenarios, the mean emissions globally were projected to decrease (Meinshausen et al., 2011). However, the changes in different areas vary dramatically. As shown in Fig. 3, there are dramatic decreasing trends for both NMVOC and $NO_x$ in both North America and Europe. In East Asia, slight increases in NMVOC occur for RCP 8.5, while decreases are seen for RCP 4.5. In India, there are predominant increasing patterns in NMVOC and $NO_x$ for both RCP 4.5 and 8.5 scenarios, which could be a major emission source region in the future. The emissions in Africa show variable increasing or decreasing patterns in different areas for both NMVOC and $NO_x$, with the NMVOC in RCP 8.5 show a particularly noticeable increasing trend.

As 2005 represents the start year of RCP scenarios in US, the 2005 US EPA's National Emission Inventory[3] was processed by Sparse Matrix Operator Kernel Emissions (SMOKE) 2.7, and then used to scale back the emissions from 2001–2004. The scaling ratios for the US emission from 2001 to 2004 are listed in Table 2, according to US EPA emissions trend data[4]. In Table 2, emissions in 2005 are listed with the unit of Tg, the emissions of the other years are listed as a ratio of the respective 2005 value. The projections of future emissions in RCP 4.5 and RCP 8.5 are based on the RCP database[5]. Biogenic emissions are highly affected by meteorological conditions used

[3] http://www.epa.gov/ttn/chief/net/2005inventory.html#inventorydata

[4] http://www.epa.gov/ttn/chief/trends/index.html#tables

[5] http://www.iiasa.ac.at/web-apps/tnt/RcpDb/dsd?Action=htmlpage&page=welcome





ACPD
13, 11315–11355, 2013



the year 2000 to, such as temperature and radiation; thus, Biogenic Emissions Inventory System (BEIS) Modeling 3.12 was used to generate hourly biogenic emissions for each year at present (2001–2004) and future (2057–2059) climate. Please note as the global chemistry CAM-Chem runs held the biogenic emissions constant between 2000 and 2050s, the emission differences between CAM-Chem and CMAQ may cause ozone differences.

As depicted in Table 2, most emissions in the US show decreasing trends in both RCP 4.5 and RCP 8.5 scenarios. By the end of 2050s, CO decreases more than 70 %; non-methane volatile organic compounds (NMVOC) and nitrogen oxides ($NO_x$) decrease by almost 70 % and 50 % in RCP 8.5, and 40 % and 60 % in RCP 4.5. In contrast, ammonia ($NH_3$) emissions increase in both scenarios, and methane ($CH_4$) emissions increase by 60 % in RCP 8.5.

## 4 Evaluation of regional model outputs

Statistical evaluation by matching observations and model outputs temporally and spatially is commonly used in retrospective studies and benchmarks have been established for evaluation criteria (USEPA, 2007). However, these statistical methods have not been used in climate studies. In global coupled climate–chemistry climate studies, zonal and monthly mean values (Young et al., 2012; Lamarque et al., 2010, 2012a) are usually compared with observations; this is due to coarse model resolutions. Previous regional air quality studies did not apply statistical evaluations due to the concern of regional climate performance (Lam et al., 2011; Nolte et al., 2008). However, regional climate modeling is able to improve the representation of climate by incorporating the high resolution topography and land use information (Gao et al., 2012). Although the boundary impact from the global climate models exists, the improved climate in regional modeling favors the paired time and space evaluation. Another important factor to consider is the emission inventory. Previous studies typically used a single year's emission inventory to represent 3-to-4 yr present conditions. For instance, Nolte at al. (2008) used the year





ACPD
13, 11315–11355, 2013



1999 to represent 1999–2003, and Lam et al. (2011) used the year 2000 to represent 1999–2001. The emissions themselves contain large biases without accounting for the inter-annual variations. We therefore take further steps to consider the emission inter-annual variations and make time- and space-paired evaluations between model outputs and observations.

In this study, we aim to document climate model performance by pairing the model outputs and observations. All the observations from US EPA Air Quality System (AQS[6]) are used to evaluate the present climate period from 2001–2004. A statistical evaluation of the pairing of the gas species (CO, $NO_2$ and $O_3$) in time and space between CMAQ outputs and AQS datasets is shown in Table 3. The benchmarks in the retrospective study (US EPA, 2007) are also listed in the Table 3. The comparison between the climate statistical metrics and the retrospective benchmarks could provide important references for future climate studies.

There are three groups of metrics: Mean Fractional Bias/Mean Fractional Error (MFB/MFE, %); Normalized Mean Bias/Normalized Mean Error (NMB/NME); and Mean Normalized Bias (MNB) and Mean Normalized Error (MNE). The equations for these six metrics are listed in the Supplement. According to US EPA (2007), the benchmarks of MFB/MFE are ±15/35 for ozone. Among all these metrics, the MFB and MFE are the least biased, and the MNB and MNE are the most biased and, thus, the least useful metrics, particularly when observation values are small. Thus, MNB and MNE are only calculated for $O_3$ with 40 and 60 ppb cut off values, according to US EPA guidelines (2007). Considering all the AQS sites at present climate condition, all statistical metrics for $O_3$ with 40 ppbv cut off meet the criteria. For $O_3$ with the 60 ppbv cut off, the absolute errors are less than 30 %, while biases for all three metrics (MFB/NMB/MNB) are slightly lower than −15 %. No benchmarks are available for CO and $NO_2$, and the biases are all less than 50 %, with most of the mean errors less than 85 %.

[6]http://www.epa.gov/ttn/airs/airsaqs/detaildata/downloadaqsdata.htm





ACPD
13, 11315–11355, 2013



The paired statistical evaluation shows strong evidence that high resolution regional downscaling could achieve reasonably good performance, particularly for MFB/MFE, with the results being comparable to the benchmarks used in the retrospective study.

## 5 Ozone concentration changes under future emission and climate conditions

### 5.1 Zonal mean vertical ozone changes from CAM-Chem

Before looking at regional air quality using CMAQ outputs, patterns of global ozone change from CAM-Chem were evaluated. The analysis of global model (CAM-Chem) uses a 10 yr period to consider inter-annual variations. Zonal mean vertical ozone changes under future climate (2050–2059) for RCP 4.5 (top panel) and RCP 8.5 (bottom panel), compared with present climate (2001–2010) were shown in Fig. 4. In both scenarios, dramatic ozone increase occurs in the high latitude areas from the upper troposphere (~ 300 hPa) to the stratosphere. The increased ozone concentrations in the high latitude stratosphere reflects the ozone recovery resulting from the reduction in halogens concentrations (Eyring et al., 2010), while the decreased ozone in tropical stratosphere is caused by the stronger Brewer–Dobson circulation (BDC) (Kawase et al., 2011; Young et al., 2012). A previous study indicates the STE could reach close to (in RCP 4.5) or more (in RCP 8.5) than twice as large as present level by the end of 21st century (Kawase et al., 2011).

For the lower troposphere, both scenarios show strong seasonal variations. In RCP 4.5 (Fig. 4, top panel), the largest ozone decrease (4 to 10 ppbv) occurs in summer and fall from mid- to high latitudes in the Northern Hemisphere (NH) across the lower-mid troposphere (surface to ~ 300 hPa). This is mainly driven by the large reductions of anthropogenic emissions in these areas and strong photochemical reactions in these two seasons. Although the same amount of emissions has been reduced, the ozone decrease in spring was not necessarily significant due to the low photochemical activity. In winter, however, a slight increase (~ 1 ppbv) was projected in the mid- to high





ACPD
13, 11315–11355, 2013



latitudes in NH, possibly resulting from the combined effects of low photochemical reaction rates and enhanced STE. The RCP 8.5 scenario (Fig. 4, bottom panel) shows widespread increasing trends in ozone levels as a result of the dramatic increase of methane emissions. The ozone concentrations undergo a larger increase in winter and spring (2–6 ppbv) than summer and fall (less than 2 ppbv) in the lower troposphere (surface to ~800 hPa). This is the result of a stronger chemical reaction and large reduction in anthropogenic emission in summer and fall than the other two seasons. The ozone increase in the mid-troposphere (800 hPa to 300 hPa) tends to show less seasonal variation, with an increase of 4–12 ppbv in the Northern Hemisphere and 2–8 ppbv in the Southern Hemisphere; while the larger increase in NH is mainly caused by larger STE and stronger BDC (Rosenlof, 1995; Young et al., 2012).

In considering the large impact of methane emissions, we conducted a sensitivity study by keeping methane emissions in 2050s at 2000 level in RCP 8.5 and compare its impact on ozone concentrations. The methane level in RCP 8.5 in 2050 is 2740 ppbv, which is 56 % higher than the level in 2000 (1751 ppbv). Compared to the RCP 8.5 with increased methane emissions, the ozone concentrations in this scenario decrease by 2–10 ppbv (Northern Hemisphere) and 0–6 ppbv (Southern Hemisphere) from surface to 300 hPa. We calculate the percentage contributions in each season as well. The largest contributions from methane emission occurs in NH from mid- to high latitude (surface to 300 hPa) in summer and fall, reaching more than 90 %, followed by spring and winter (reaches 60–80 %). This contributes evidence to the theory that methane emissions are the major factor leading to ozone increase in the summer and fall, relative to the more active photochemical reactions during these seasons. However, in spring and winter, 20–40 % of ozone increases are contributed by other factors, such as the increased stratosphere-troposphere exchange (STE) (Kawase et al., 2011).

### 5.2 Seasonal variations of surface ozone concentrations by the end of 2050s

After evaluating the global zonal mean ozone changes, we focus on the surface ozone changes in the continental US from regional downscaling simulations. Figure 5 shows





ACPD
13, 11315–11355, 2013



seasonal mean surface ozone differences by the end of 2050s (2057–2059) compared with the present (2001–2004). Under RCP 4.5 scenario, by the end of 2050s, in spring, summer, and fall (Fig. 5a–c), significant decreases in ozone concentrations occur across most of US, resulting from ozone emission precursor reductions (Table 2). In summer, when photochemical reactions are the most active, the large ozone precursor emissions reduction leads to the largest decrease of ozone concentrations, ranging from 6 to 10 ppbv. However, a few exceptions occur near major cities, including Seattle (WA), San Francisco (CA), Los Angeles (CA), Phoenix (AZ), Denver (CO), Chicago (IL), New York City (NY) and Atlanta (GA), etc., with ozone increases of 3 to 7 ppbv. The ozone increases, particularly in spring (Fig. 5a), fall (Fig. 5c) and winter (Fig. 5d), in the major cities are mainly due to NO titration by reducing a large percentage of $NO_x$ emissions (~ 65 % from Table 2). In summer (Fig. 5b), these cities do not show as large an increase as other seasons, largely due to the compensation between less NO titration and reduced photochemical reactions resulting from emission reductions. As a result of low chemical reactivity, titration plays a major role in ozone loss in winter; thus, reducing $NO_x$ leads to large areas of ozone increase (Fig. 5d).

In the RCP 8.5 scenario, the ozone increase by 3 to 7 ppbv in major cities is similarly driven by weakened NO titration as RCP 4.5. However, compared with RCP 4.5, RCP 8.5 results show some obvious differences. In spring (Fig. 5e), there are 3–6 ppbv increases in the western and Midwestern US as well as large areas of Canada. In summer (Fig. 5f) and fall (Fig. 5g), the northwestern domain area shows an increasing trends of 2–4 ppbv. In winter (Fig. 5h), ozone concentrations increase across nearly the entire domain, ranging from 3 to 10 ppbv.

Considering the large differences between RCP 4.5 and RCP 8.5 in the northwest (Fig. 5a vs. 5e) and most of the domain (Fig. 5d vs. 5h), we conducted a sensitivity study to explore the possible causes. For the RCP 8.5 scenario, while keeping all other factors constant, the boundary conditions for regional chemistry model CMAQ were changed to present conditions (2001–2004) instead of using future conditions (2057–2059). This new scenario was named RCP8.5_BDY. The ozone differences between





ACPD
13, 11315–11355, 2013



this scenario and the present condition were shown in Fig. 5i–l. Compared with Fig. 5e–g, the high ozone increase in the western boundary disappears in spring (Fig. 5i), while the increases in the northwest and southeast areas in summer and fall disappear as well (Fig. 5j and k). In winter, sizeable areas do not show increases after applying the present low boundary concentrations (Fig. 5l), and the ozone spatial patterns are similar to Fig. 5d under RCP 4.5. This commonality in both RCP 4.5 and RCP 8.5 scenarios further demonstrates the ozone increase in winter near major cities and parts of the northeastern US is not due to the boundary impact or methane increase, but instead, likely results from the NO titration effect.

The new scenario (RCP8.5_BDY) suggests a much larger impact from the boundary in winter under RCP 8.5. This impact can be further explained by the bottom panel of Fig. 4. As discussed in the Sect. 4.1, the lower troposphere in NH in the mid- to high latitude shows the highest increase in winter, due to the increased methane emissions, the recovery of ozone in the stratosphere and higher STE in RCP 8.5. Additionally, inter-continental transport could also play an important role considering the different projections of ozone emission precursors in different continents (Young et al., 2012; Fiore et al., 2009; Wild et al., 2012).

## 6 Maximum daily 8 h ozone changes in nine climate regions in US

### 6.1 Maximum daily 8 h ozone under future climate

In addition to the seasonal average ozone changes across the entire continental domain, we focus more on air quality in the nine climate regions in US from the downscaling results. Cumulative distributions of Maximum daily 8 h ozone (MDA8) for present climate (2001–2004) and future climate (RCP 4.5 and RCP 8.5, 2057–2059) was shown in Fig. 6. Overall, compared with present climate, the cumulative distribution of RCP 4.5 shifts to the lower values, indicating reduced ozone concentrations under the emission reduction scenario RCP 4.5. Comparing RCP 4.5 with RCP 8.5, the right shift





ACPD
13, 11315–11355, 2013



of distribution for RCP 8.5 indicates higher ozone concentrations under this scenario. In RCP 8.5, the northeast, southeast, central and south show decreasing patterns in the high ozone concentration levels, (i.e., higher than 50–60 ppbv), yet increasing patterns in the low ozone concentration levels, (i.e., from 20 ppbv to 50 ppbv). However, the northwest, west and west north central show increasing patterns in the ozone level from 30 ppbv to 60 ppbv, little change in the level higher than 60 ppbv to 70 ppbv. The difference in ozone change patterns between eastern and western US could be attributed to different ozone precursor emission distributions (Fig. 3a, b). Figure 3a and b showed more dense emission distributions in the eastern US than the western US. Note there were 10 ppbv or larger differences as described earlier (the eastern US shows increasing patterns in the ozone level from 20–50 ppbv, while the western US shows 30–60 ppbv). As is explained in Fig. 5e–h, the ozone increase in RCP 8.5 mainly occurs in spring and winter when the ozone photochemical reactions are not the major driver; the higher background ozone (10–15 ppbv higher in the western than the eastern US, Zhang et al., 2011), higher elevation and stratosphere intrusion play key roles in driving the differences.

In addition to the cumulative distributions, the percentage of MDA8 exceeding 60 and 75 ppbv is also listed in Fig. 6. The National Ambient Air Quality Standards (NAAQS) for MDA8 has been 75 ppbv since 2008. As the NAAQS might become more stringent in the future, the 60 ppbv was listed to provide potentially useful information in the years to come. The negative numbers in Fig. 6 indicate ozone exceedance decreases in the future compared with present climate. From Fig. 6, we find that all blue numbers (second row) are negative, indicating ozone concentration decreases in RCP 4.5. However, in RCP 8.5, the exceedance of 60 ppbv increases by 3 % to 10 % in the western US, with the highest increase in the northwest due to increased STE, methane emissions and possibly intercontinental transport; the exceedances in the eastern US decrease by 2 % to 14 %, resulting from large anthropogenic emission reductions in the emission dense area, smaller STE and less intercontinental impact.





ACPD
13, 11315–11355, 2013



### 6.2 The changes of Potential Vorticity (PV) at 500 hPa

To further evaluate the STE under RCP 8.5, Potential Vorticity (PV) in mid-troposphere (500 hPa) was analyzed, and is shown in Fig. 7. The analysis indicates a mean increase over the northwestern US and Canada in 2050s compared to present climate (2000s).This increase is an indication of stronger penetration of stratospheric intrusion and may therefore partially explain the increase of ozone concentrations in winter in Figs. 5h and 6. In spring, the PV in the western US is relatively stronger in 2050s as well, although to a lesser extent. This may also contribute to the corresponding higher ozone concentrations in spring as shown in Figs. 5e and 6. Changes to PV in other seasons and regions of the United States do not appear to be large enough to warrant a significant impact on tropospheric ozone.

## 7 More intense heat waves and its impact on air quality

### 7.1 Heat wave duration and frequency

Until now, studies of climate impact on air quality have focused on the comparison between different climate scenarios or different emissions scenarios (Kawase et al., 2011; Lam et al., 2011; Nolte et al., 2008). However, under the same scenario, different meteorological conditions, in particular a heat wave period, could potentially increase ozone levels (Stedman, 2004). This is a very important concern, particularly for control strategies and policies. Thus, we investigate heat waves under future climate and further evaluate the impact of heat waves on ozone.

Two metrics of heat waves were used in this study: duration (number of days for each heat wave) and frequency (number of heat waves). Daily maximum temperature was used to define a heat wave. It is defined as the longest period that meets the following two criteria: (1) the maximum daily temperature has to reach 97.5th percentile of the entire period (2001–2004 in this case) for three or more consecutive days; and





ACPD
13, 11315–11355, 2013



(2) during this period, the mean daily maximum temperature is no lower than 97.5th percentile, and for each day, the daily maximum temperature has to be equal to or higher than the 81st percentile (Huth et al., 2000; Meehl and Tebaldi, 2004; Gao et al., 2012). Definitions of future heat waves use the same thresholds in order to compare the changes between present and future climate.

Figure 8 shows the heat wave duration and frequency at present and future climate. At present (Fig. 8a, b), the heat wave duration ranges from 3.7 to 4.4 days per event, and the number of annual heat wave events are 1 to 1.5. In RCP 4.5 (Fig. 8c,d), by the end of 2050s, most of the regions show increasing trends for heat wave duration, except central and upper midwest, which show slight decreases. The mean increase of duration across the entire US is 23 %, while the largest increase of 68 % occurs in the southwest. For the annual number of events, all regions show increasing patterns, with a mean increase in US of 131 %. The frequency in the northeast and northwest is more than triple compared with present climate. Far more intense heat waves are projected to occur in RCP 8.5 (Fig. 8e, f), with mean increase of 54 % and 313 % for duration and frequency, more than twice as high as the increase in RCP 4.5 (23 % and 131 %). The duration increase ranges from 29 % to 90 % among the 9 regions. The increase of events is more significant, with a minimum increase of 173 % in the west and a maximum increase of 564 % in the northeast.

### 7.2 Impact of heat waves on MDA8 ozone concentrations

The heat waves discussed above most occur from June to October; we therefore investigated the impact of heat waves during these five months. Figure 9 shows the MDA8 distributions during heat wave period and other days (no heat waves) from June to October. In both RCP 4.5 and RCP 8.5, the majority of the regions show right shifts of MDA8 distribution during the heat wave period, which pushes the higher MDA8 values accounting for a larger percentage. Three regions, including the southeast, central and Upper Midwest, were projected to have less impact on ozone from heat waves in both scenarios. This phenomenon can be explained by Fig. 8c–f. In RCP 4.5 (Fig. 8c, d), the





ACPD
13, 11315–11355, 2013



annual heat wave events (heat wave frequency) for these three regions are less than 3 and the mean annual events in the central is only 1.7. In the southeast, even though the mean annual events are 3.1, in fact most of the states in this region show events around 1.0, except Florida. The reason Florida shows a higher number of events is due to its position adjacent to the ocean and its small diurnal temperature variations; small diurnal variations favor the number of heat wave events in terms of percentile determination methodology. Thus, the southeast did not have a high impact of heat waves on MDA8 ozone. In RCP 8.5, although the heat wave duration and frequency in three regions (southeast, central and upper midwest) (Fig. 8e, f) are not that small, other regions in the western regions (northwest, west, southwest, west north central, south) show much longer durations (more than 10 days/event), and the northeast has a frequency of more than 10 events per year.

In addition to the distributions, Fig. 9 also lists the differences in mean MDA8 ozone (bottom row), MDA8 ozone exceeding 60 ppbv (middle row) and 75 ppbv (top row) for both RCP 4.5 and RCP 8.5 scenarios. In RCP 8.5, three western regions, west north central, west, and southwest, are projected to have more than 8 ppbv of MDA8 during the heat wave days than other days, indicating a dramatic impact heat waves exert on ozone. Correspondingly, more than 30 % (or 10 %) during the heat wave days have MDA8 exceeding 60 ppbv (or 75 ppbv) in the three western regions (west north central, west, and southwest) than other days.

## 8 Conclusions

Evaluating model simulations results is an important step before pursuing any future projections. By applying high resolution topography, land use information and accurate emission inventory, it is possible to conduct time- and space-paired statistical evaluation on climate–chemistry simulations. This study showed strong confidence that the statistical metrics, commonly used in retrospective studies, can be applied to climate–chemistry studies; and the benchmarks in the retrospective studies could be applied





ACPD
13, 11315–11355, 2013



to the climate–chemistry studies, or with slight relaxation. Of course, more climate–chemistry studies are needed, albeit provided that when computational resources are available, to further evaluate these statistical metrics and thus build comprehensive benchmarks for regional climate–chemistry evaluation.

In future climate conditions, including both RCP 4.5 and RCP 8.5, the ozone recovery in stratosphere and increased stratosphere–troposphere exchange (STE) leads to dramatic ozone increase from the upper troposphere (~ 300 hPa) to stratosphere. In the lower troposphere, ozone change patterns show seasonal variations. In RCP 4.5, the largest decrease occurs in summer and fall, while small changes occur in spring and winter, and are mainly driven by the photochemical reactivity seasonal differences. RCP 8.5 scenario shows consistent seasonal variations. However, with the large increase of methane emissions, instead of decrease, it shows increasing trends of ozone concentrations. The lowest increase occurs in summer and largest increase occurs in winter.

The dynamical downscaling results are used to explore more details in continental US. By the end of 2050s, RCP 4.5 scenario shows significant decreases in ozone concentrations across most of US. However, a few major cities show dramatic ozone increases due to NO titrations. In particular, in winter with low chemical reactivity, titration plays a major role in ozone loss. Therefore, reducing $NO_x$ could lead to large areas of ozone increase. Compared with RCP 4.5, RCP 8.5 shows consistent NO titration effect; but when combined with increased methane emissions, leads to a much less dramatic reduction or even increase in ozone. These two scenarios confirm that the reduction of methane emissions will undoubtedly benefit future ozone control. However, the titration effect in major cities with dense population cannot be ignored and reasonable control of $NO_x$ should be implemented.

Another important issue discussed in this study was the heat wave effect and its impact on ozone concentrations. Our results show significant impact of heat waves on MDA8 ozone. Much more intense heat waves, including both in duration and frequency, were projected to occur in RCP 8.5. The western US, encompassing the northwest,





ACPD
13, 11315–11355, 2013



west, southwest, west north central, and south, was projected to have long heat wave durations (more than 10 days/event); and the northeast was projected to have more than 10 events per year. These heat waves lead to 8 ppbv in the western US and close to 6 ppbv in the northeast higher of MDA8 ozone than other days without heat waves. These findings addresses important issues regarding future air quality control, indicating that the ozone may be better controlled by reducing both ozone precursor emission and greenhouse gases emission.

**Supplementary material related to this article is available online at: http://www.atmos-chem-phys-discuss.net/13/11315/2013/acpd-13-11315-2013-supplement.pdf.**

*Acknowledgements.* Model simulations of this research were partially supported by the National Science Foundation through TeraGrid resources provided by National Institute for Computational Sciences (NICS) (TG-ATM110009 and UT-TENN0006). It also used resources of the Oak Ridge Leadership Computing Facility at the Oak Ridge National Laboratory, which is supported by the Office of Science of the US Department of Energy (Contract No. DE-AC05-00OR22725). Data analysis was sponsored by the Climate and Health program led by George Luber at the Centers for Disease Control and Prevention (CDC) (5 U01 EH000405). The CESM project is supported by the National Science Foundation and the Office of Science (BER) of the US Department of Energy. The National Center for Atmospheric Research is operated by the University Corporation for Atmospheric Research under sponsorship of the National Science Foundation.

## References

Aghedo, A. M., Bowman, K. W., Worden, H. M., Kulawik, S. S., Shindell, D. T., Lamarque, J. F., Faluvegi, G., Parrington, M., Jones, D. B. A., and Rast, S.: The vertical distribution of ozone instantaneous radiative forcing from satellite and chemistry climate models, J. Geophys. Res., 116, D01305, doi:10.1029/2010jd014243, 2011.





ACPD
13, 11315–11355, 2013



Annan, J. D. and Hargreaves, J. C.: Understanding the CMIP3 multimodel ensemble, J. Climate, 24, 4529–4538, doi:10.1175/2011jcli3873.1, 2011.
Bell, M., Goldberg, R., Hogrefe, C., Kinney, P., Knowlton, K., Lynn, B., Rosenthal, J., Rosenzweig, C., and Patz, J.: Climate change, ambient ozone, and health in 50 US cities, Climatic Change, 82, 61–76, doi:10.1007/s10584-006-9166-7, 2007.
Byun, D. and Schere, K. L.: Review of the governing equations, computational algorithms, and other components of the models-3 Community Multiscale Air Quality (CMAQ) modeling system, Appl. Mech. Rev., 59, 51–77, doi:10.1115/1.2128636, 2006.
Caldwell, P., Chin, H.-N. S., Bader, D. C., and and Bala, G.: Evaluation of a WRF dynamical downscaling simulation over California, Climatic Change, 95, 499–521, doi:10.1007/s10584-009-9583-5, 2009.
Carlton, A. G., Bhave, P. V., Napelenok, S. L., Edney, E. O., Sarwar, G., Pinder, R. W., Pouliot, G. A., and Houyoux, M.: Model representation of secondary organic aerosol in CMAQv4.7, Environ. Sci. Technol., 44, 8553–8560, doi:10.1021/es100636q, 2010.
Chen, F. and Dudhia, J.: Coupling an advanced land surface-hydrology model with the Penn State-NCAR MM5 modeling system, part I: model implementation and sensitivity, Mon. Weather Rev., 129, 569–585, doi:10.1175/1520-0493(2001)129<0569:caalsh>2.0.co;2, 2001.
Emmons, L. K., Walters, S., Hess, P. G., Lamarque, J.-F., Pfister, G. G., Fillmore, D., Granier, C., Guenther, A., Kinnison, D., Laepple, T., Orlando, J., Tie, X., Tyndall, G., Wiedinmyer, C., Baughcum, S. L., and Kloster, S.: Description and evaluation of the Model for Ozone and Related chemical Tracers, version 4 (MOZART-4), Geosci. Model Dev., 3, 43–67, doi:10.5194/gmd-3-43-2010, 2010.
Eyring, V., Cionni, I., Bodeker, G. E., Charlton-Perez, A. J., Kinnison, D. E., Scinocca, J. F., Waugh, D. W., Akiyoshi, H., Bekki, S., Chipperfield, M. P., Dameris, M., Dhomse, S., Frith, S. M., Garny, H., Gettelman, A., Kubin, A., Langematz, U., Mancini, E., Marchand, M., Nakamura, T., Oman, L. D., Pawson, S., Pitari, G., Plummer, D. A., Rozanov, E., Shepherd, T. G., Shibata, K., Tian, W., Braesicke, P., Hardiman, S. C., Lamarque, J. F., Morgenstern, O., Pyle, J. A., Smale, D., and Yamashita, Y.: Multi-model assessment of stratospheric ozone return dates and ozone recovery in CCMVal-2 models, Atmos. Chem. Phys., 10, 9451–9472, doi:10.5194/acp-10-9451-2010, 2010.
Fiore, A. M., Dentener, F. J., Wild, O., Cuvelier, C., Schultz, M. G., Hess, P., Textor, C., Schulz, M., Doherty, R. M., Horowitz, L. W., MacKenzie, I. A., Sanderson, M. G.,





ACPD
13, 11315–11355, 2013



Shindell, D. T., Stevenson, D. S., Szopa, S., Van Dingenen, R., Zeng, G., Atherton, C., Bergmann, D., Bey, I., Carmichael, G., Collins, W. J., Duncan, B. N., Faluvegi, G., Folberth, G., Gauss, M., Gong, S., Hauglustaine, D., Holloway, T., Isaksen, I. S. A., Jacob, D. J., Jonson, J. E., Kaminski, J. W., Keating, T. J., Lupu, A., Marmer, E., Montanaro, V., Park, R. J., Pitari, G., Pringle, K. J., Pyle, J. A., Schroeder, S., Vivanco, M. G., Wind, P., Wojcik, G., Wu, S., and Zuber, A.: Multimodel estimates of intercontinental source-receptor relationships for ozone pollution, J. Geophys. Res., 114, D04301, doi:10.1029/2008jd010816, 2009.

Fiore, A. M., Naik, V., Spracklen, D. V., Steiner, A., Unger, N., Prather, M., Bergmann, D., Cameron-Smith, P. J., Cionni, I., Collins, W. J., Dalsoren, S., Eyring, V., Folberth, G. A., Ginoux, P., Horowitz, L. W., Josse, B., Lamarque, J.-F., MacKenzie, I. A., Nagashima, T., O'Connor, F. M., Righi, M., Rumbold, S. T., Shindell, D. T., Skeie, R. B., Sudo, K., Szopa, S., Takemura, T., and Zeng, G.: Global air quality and climate, Chem. Soc. Rev., 41, 6663–6683, 2012.

Fu, J. S., Dong, X., Gao, Y., Wong, D. C., and Lam, Y. F.: Sensitivity and linearity analysis of ozone in East Asia: the effects of domestic emission and intercontinental transport, J. Air Waste Manage., 62, 1102–1114, doi:10.1080/10962247.2012.699014, 2012a.

Fu, J. S., Hsu, N. C., Gao, Y., Huang, K., Li, C., Lin, N.-H., and Tsay, S.-C.: Evaluating the influences of biomass burning during 2006 BASE-ASIA: a regional chemical transport modeling, Atmos. Chem. Phys., 12, 3837–3855, doi:10.5194/acp-12-3837-2012, 2012b.

Ganguly, A. R., Steinhaeuser, K., Erickson, D. J., Branstetter, M., Parish, E. S., Singh, N., Drake, J. B., and Buja, L.: Higher trends but larger uncertainty and geographic variability in 21st century temperature and heat waves, P. Natl. Acad. Sci. USA, 106, 15555–15559, 2009.

Gao, Y., Fu, J. S., Drake, J. B., Liu, Y., and Lamarque, J.-F.: Projected changes of extreme weather events in the eastern United States based on a high-resolution climate modeling system, Environ. Res. Lett., 7, 044025, doi:10.1088/1748-9326/7/4/044025, 2012.

Hong, S.-Y. and Lim, J.-O.: The WRF Single-Moment 6-Class Microphysics Scheme (WSM6), J. Korean Meteor. Soc., 42, 129–151, 2006.

Huang, H.-C., Lin, J., Tao, Z., Choi, H., Patten, K., Kunkel, K., Xu, M., Zhu, J., Liang, X.-Z., Williams, A., Caughey, M., Wuebbles, D. J., and Wang, J.: Impacts of long-range transport of global pollutants and precursor gases on US air quality under future climatic conditions, J. Geophys. Res., 113, D19307, doi:10.1029/2007jd009469, 2008.





ACPD
13, 11315–11355, 2013



Huang, K., Fu, J. S., Hsu, N. C., Gao, Y., Dong, X., Tsay, S.-C., and Lam, Y. F.: Impact assessment of biomass burning on air quality in southeast and east Asia during BASE-ASIA, Atmos. Environ., doi:10.1016/j.atmosenv.2012.03.048, in press, 2012.
Hunke, E. C. and Lipscomb, W. H.: CICE: the Los Alamos Sea Ice Model, documentation and software, version 4.0, Los Alamos National Laboratory Tech. Rep. LA-CC-06-012, 2008.
Huth, R., Kysely, J., and Pokorna, L.: GCM simulation of heat waves, dry spells, and their relationships to circulation, Climatic Change, 46, 29–60, 2000.
Iacono, M. J., Delamere, J. S., Mlawer, E. J., Shephard, M. W., Clough, S. A., and Collins, W. D.: Radiative forcing by long-lived greenhouse gases: calculations with the AER radiative transfer models, J. Geophys. Res., 113, D13103, doi:10.1029/2008jd009944, 2008.
Jacob, D. J. and Winner, D. A.: Effect of climate change on air quality, Atmos. Environ., 43, 51–63, doi:10.1016/j.atmosenv.2008.09.051, 2009.
Janjić, Z. I.: The Step-Mountain Coordinate: physical package, Mon. Weather Rev., 118, 1429–1443, doi:10.1175/1520-0493(1990)118<1429:tsmcpp>2.0.co;2, 1990.
Judah, L. C., Jason, C. F., Mathew, A. B., Vladimir, A. A., and Jessica, E. C.: Arctic warming, increasing snow cover and widespread boreal winter cooling, Environ. Res. Lett., 7, 014007, doi:10.1088/1748-9326/7/1/014007, 2012.
Kain, J. S.: The Kain–Fritsch convective parameterization: an update, J. Appl. Meteorol., 43, 170–181, doi:10.1175/1520-0450(2004)043<0170:tkcpau>2.0.co;2, 2004.
Kawase, H., Nagashima, T., Sudo, K., and Nozawa, T.: Future changes in tropospheric ozone under Representative Concentration Pathways (RCPs), Geophys. Res. Lett., 38, L05801, doi:10.1029/2010gl046402, 2011.
Kelly, J., Makar, P. A., and Plummer, D. A.: Projections of mid-century summer air-quality for North America: effects of changes in climate and precursor emissions, Atmos. Chem. Phys., 12, 5367–5390, doi:10.5194/acp-12-5367-2012, 2012.
Knutti, R. and Sedlacek, J.: Robustness and uncertainties in the new CMIP5 climate model projections, Nature Clim. Change, 3, 369–373, doi:10.1038/nclimate1716, 2013.
Lam, Y. F. and Fu, J. S.: A novel downscaling technique for the linkage of global and regional air quality modeling, Atmos. Chem. Phys., 9, 9169–9185, doi:10.5194/acp-9-9169-2009, 2009.
Lam, Y. F., Fu, J. S., Wu, S., and Mickley, L. J.: Impacts of future climate change and effects of biogenic emissions on surface ozone and particulate matter concentrations in the United States, Atmos. Chem. Phys., 11, 4789–4806, doi:10.5194/acp-11-4789-2011, 2011.





ACPD
13, 11315–11355, 2013



Lamarque, J.-F. and Solomon, S.: Impact of changes in climate and halocarbons on recent lower stratosphere ozone and temperature trends, J. Climate, 23, 2599–2611, doi:10.1175/2010jcli3179.1, 2010.

Lamarque, J.-F., Bond, T. C., Eyring, V., Granier, C., Heil, A., Klimont, Z., Lee, D., Liousse, C., Mieville, A., Owen, B., Schultz, M. G., Shindell, D., Smith, S. J., Stehfest, E., Van Aardenne, J., Cooper, O. R., Kainuma, M., Mahowald, N., McConnell, J. R., Naik, V., Riahi, K., and van Vuuren, D. P.: Historical (1850–2000) gridded anthropogenic and biomass burning emissions of reactive gases and aerosols: methodology and application, Atmos. Chem. Phys., 10, 7017–7039, doi:10.5194/acp-10-7017-2010, 2010.

Lamarque, J.-F., Kyle, G., Meinshausen, M., Riahi, K., Smith, S., van Vuuren, D., Conley, A., and Vitt, F.: Global and regional evolution of short-lived radiatively-active gases and aerosols in the Representative Concentration Pathways, Climatic Change, 109, 191–212, doi:10.1007/s10584-011-0155-0, 2011a.

Lamarque, J.-F., McConnell, J. R., Shindell, D. T., Orlando, J. J., and Tyndall, G. S.: Understanding the drivers for the 20th century change of hydrogen peroxide in Antarctic ice-cores, Geophys. Res. Lett., 38, L04810, doi:10.1029/2010gl045992, 2011b.

Lamarque, J.-F., Emmons, L. K., Hess, P. G., Kinnison, D. E., Tilmes, S., Vitt, F., Heald, C. L., Holland, E. A., Lauritzen, P. H., Neu, J., Orlando, J. J., Rasch, P. J., and Tyndall, G. K.: CAM-chem: description and evaluation of interactive atmospheric chemistry in the Community Earth System Model, Geosci. Model Dev., 5, 369–411, doi:10.5194/gmd-5-369-2012, 2012.

Lamarque, J.-F., Shindell, D. T., Josse, B., Young, P. J., Cionni, I., Eyring, V., Bergmann, D., Cameron-Smith, P., Collins, W. J., Doherty, R., Dalsoren, S., Faluvegi, G., Folberth, G., Ghan, S. J., Horowitz, L. W., Lee, Y. H., MacKenzie, I. A., Nagashima, T., Naik, V., Plummer, D., Righi, M., Rumbold, S. T., Schulz, M., Skeie, R. B., Stevenson, D. S., Strode, S., Sudo, K., Szopa, S., Voulgarakis, A., and Zeng, G.: The Atmospheric Chemistry and Climate Model Intercomparison Project (ACCMIP): overview and description of models, simulations and climate diagnostics, Geosci. Model Dev., 6, 179–206, doi:10.5194/gmd-6-179-2013, 2013.

Mass, C. F., Ovens, D., Westrick, K., and Colle, B. A.: Does increasing horizontal resolution produce more skillful forecasts?, B. Am. Meteorol. Soc., 83, 407–430, doi:10.1175/1520-0477(2002)083<0407:dihrpm>2.3.co;2, 2002.

Meehl, G. A. and Tebaldi, C.: More intense, more frequent, and longer lasting heat waves in the 21st century, Science, 305, 994–997, 2004.





ACPD
13, 11315–11355, 2013



Meehl, G. A., Covey, C., McAvaney, B., Latif, M., and Stouffer, R. J.: Overview of the coupled model intercomparison project, B. Am. Meteorol. Soc., 86, 89–93, doi:10.1175/bams-86-1-89, 2005.

Meehl, G. A., Covey, C., Taylor, K. E., Delworth, T., Stouffer, R. J., Latif, M., McAvaney, B., and Mitchell, J. F. B.: The WCRP CMIP3 Multimodel Dataset: a new era in climate change research, B. Am. Meteorol. Soc., 88, 1383–1394, doi:10.1175/bams-88-9-1383, 2007.

Meehl, G. A., Washington, W. M., Arblaster, J. M., Hu, A., Teng, H., Tebaldi, C., Sanderson, B. N., Lamarque, J.-F., Conley, A., Strand, W. G., and White, J. B.: Climate system response to external forcings and climate change projections in CCSM4, J. Climate, 25, 3661–3683, doi:10.1175/jcli-d-11-00240.1, 2011.

Meinshausen, M., Smith, S. J., Calvin, K., Daniel, J. S., Kainuma, M. L. T., Lamarque, J. F., Matsumoto, K., Montzka, S. A., Raper, S. C. B., Riahi, K., Thomson, A., Velders, G. J. M., and Vuuren, D. P. P.: The RCP greenhouse gas concentrations and their extensions from 1765 to 2300, Climatic Change, 109, 213–241, doi:10.1007/s10584-011-0156-z, 2011.

Mellor, G. L. and Yamada, T.: Development of a turbulence closure-model for geophysical fluid problems, Rev. Geophys., 20, 851–875, 1982.

Morcrette, J. J., Barker, H. W., Cole, J. N. S., Iacono, M. J., and Pincus, R.: Impact of a new radiation package, McRad, in the ECMWF Integrated Forecasting System, Mon. Weather Rev., 136, 4773–4798, doi:10.1175/2008mwr2363.1, 2008.

Moss, R. H., Edmonds, J. A., Hibbard, K. A., Manning, M. R., Rose, S. K., van Vuuren, D. P., Carter, T. R., Emori, S., Kainuma, M., Kram, T., Meehl, G. A., Mitchell, J. F. B., Nakicenovic, N., Riahi, K., Smith, S. J., Stouffer, R. J., Thomson, A. M., Weyant, J. P., and Wilbanks, T. J.: The next generation of scenarios for climate change research and assessment, Nature, 463, 747–756, 2010.

Nakicenovic, N. and Swart, R.: Special report on emissions scenarios: a special report of working group III of the Intergovernmental Panel on Climate Change, Cambridge University Press, Cambridge, UK and New York, NY, USA, 2000.

Neale, R. B., Richter, J. H., Conley, A. J., Park, S., Lauritzen, P. H., Gettelman, A., Williamson, D. L., Rasch, P. J., Vavrus, S. J., Taylor, M. A., Collins, W. D., Zhang, M., and Lin, S.-J.: Description of the NCAR Community Atmosphere Model (CAM 4.0), NCAR Tech. Note NCAR/TN-XXX+STR (Draft), National Center for Atmospheric Research, Boulder, Colorado, USA, 194 pp., 2010.





ACPD
13, 11315–11355, 2013



Nolte, C. G., Gilliland, A. B., Hogrefe, C., and Mickley, L. J.: Linking global to regional models to assess future climate impacts on surface ozone levels in the United States, J. Geophys. Res., 113, D14307, doi:10.1029/2007jd008497, 2008.

Oleson, K. W., Lawrence, D. M., Bonan, G. B., Flanner, M. G., Kluzek, E., Lawrence, P. J., Levis, S., Swenson, S. C., Thornton, P. E., Dai, A., Decker, M., Dickinson, R., Feddema, J., Heald, C. L., Hoffman, F., Lamarque, J.-F., Mahowald, N., Niu, G.-Y., Qian, T., Randerson, J., Running, S., Sakaguchi, K., Slater, A., Stockli, R., Wang, A., Yang, Z.-L., Zeng, X., and Zeng, X.: Technical Description of version 4.0 of the Community Land Model (CLM), NCAR Technical Note NCAR/TN-478+STR, National Center for Atmospheric Research, Boulder, CO, 257 pp., 2010.

Otte, T. L. and Pleim, J. E.: The Meteorology-Chemistry Interface Processor (MCIP) for the CMAQ modeling system: updates through MCIPv3.4.1, Geosci. Model Dev., 3, 243–256, doi:10.5194/gmd-3-243-2010, 2010.

Riahi, K., Grübler, A., and Nakicenovic, N.: Scenarios of long-term socio-economic and environmental development under climate stabilization, Technol. Forecast. Soc., 74, 887–935, doi:10.1016/j.techfore.2006.05.026, 2007.

Rogelj, J., Meinshausen, M., and Knutti, R.: Global warming under old and new scenarios using IPCC climate sensitivity range estimates, Nature Clim. Change, 2, 248–253, doi:10.1038/nclimate1385, 2012.

Rosenlof, K. H.: Seasonal cycle of the residual mean meridional circulation in the stratosphere, J. Geophys. Res., 100, 5173–5191, doi:10.1029/94jd03122, 1995.

Skamarock, W. C. and Klemp, J. B.: A time-split nonhydrostatic atmospheric model for weather research and forecasting applications, J. Comput. Phys., 227, 3465–3485, doi:10.1016/j.jcp.2007.01.037, 2008.

Smith, R., Jones, P., Briegleb, B., Bryan, F., Danabasoglu, G., Dennis, J., Dukowicz, J., Eden C., Fox-Kemper, B., Gent, P., Hecht, M., Jayne, S., Jochum, M., Large, W., Lindsay, K., Maltrud, M., Norton, N., Peacock, S., Vertenstein, M., and Yeager, S.: The Parallel Ocean Program (POP) reference manual, Ocean Component of the Community Climate System Model (CCSM) and Community Earth System Model (CESM), Los Alamos National Laboratory Tech. Rep. LAUR-10-01853, 2010.

Smith, S. J. and Wigley, T. M. L.: Multi-gas forcing stabilization with the MiniCAM, Energ. J., 373–391, 2006.





ACPD
13, 11315–11355, 2013



Solomon, S., Qin, D., Manning, M., Marquis, M., Averyt, K., Tignor, M., Miller, H. L., and Chen, Z.: IPCC 2007 Climate Change 2007: the physical science basis, contribution of working group I to the fourth assessment report of the Intergovernmental Panel on Climate Change, Cambridge University Press, Cambridge, 2007.

Stedman, J. R.: The predicted number of air pollution related deaths in the UK during the August 2003 heatwave, Atmos. Environ., 38, 1087–1090, doi:10.1016/j.atmosenv.2003.11.011, 2004.

Stroeve, J. C., Kattsov, V., Barrett, A., Serreze, M., Pavlova, T., Holland, M., and Meier, W. N.: Trends in Arctic sea ice extent from CMIP5, CMIP3 and observations, Geophys. Res. Lett., 39, L16502, doi:10.1029/2012GL052676, 2012

Taylor, K. E., Stouffer, R. J., and Meehl, G. A.: A Summary of the CMIP5 Experiment Design, available at: http://www-pcmdi.llnl.gov/, 2009.

Taylor, K. E., Stouffer, R. J., and Meehl, G. A.: An overview of CMIP5 and the experiment design, Bull. Am. Meteorol. Soc., 93, 485–498, doi:10.1175/bams-d-11-00094.1, 2012.

USEPA: Guidance on the Use of Models and Other Analyses for Demonstrating Attainment of Air Quality Goals for Ozone, $PM_{2.5}$ and Regional Haze, EPA-454/B-07e002, 2007.

Vieno, M., Dore, A. J., Stevenson, D. S., Doherty, R., Heal, M. R., Reis, S., Hallsworth, S., Tarrason, L., Wind, P., Fowler, D., Simpson, D., and Sutton, M. A.: Modelling surface ozone during the 2003 heat-wave in the UK, Atmos. Chem. Phys., 10, 7963–7978, doi:10.5194/acp-10-7963-2010, 2010.

Wild, O., Fiore, A. M., Shindell, D. T., Doherty, R. M., Collins, W. J., Dentener, F. J., Schultz, M. G., Gong, S., MacKenzie, I. A., Zeng, G., Hess, P., Duncan, B. N., Bergmann, D. J., Szopa, S., Jonson, J. E., Keating, T. J., and Zuber, A.: Modelling future changes in surface ozone: a parameterized approach, Atmos. Chem. Phys., 12, 2037–2054, doi:10.5194/acp-12-2037-2012, 2012.

Wise, M., Calvin, K., Thomson, A., Clarke, L., Bond-Lamberty, B., Sands, R., Smith, S. J., Janetos, A., and Edmonds, J.: Implications of limiting $CO_2$ concentrations for land use and energy, Science, 324, 1183–1186, doi:10.1126/science.1168475, 2009.

Wong, D. C., Pleim, J., Mathur, R., Binkowski, F., Otte, T., Gilliam, R., Pouliot, G., Xiu, A., Young, J. O., and Kang, D.: WRF-CMAQ two-way coupled system with aerosol feedback: software development and preliminary results, Geosci. Model Dev., 5, 299–312, doi:10.5194/gmd-5-299-2012, 2012.





ACPD
13, 11315–11355, 2013



Yarwood, G., Rao, S., Yocke, M., and Whitten, G.: Updates to the Carbon Bond Chemical Mechanism: CB05, US Environmental Protection Agency, Research Triangle Park, NC, 2005.

Young, P. J., Archibald, A. T., Bowman, K. W., Lamarque, J.-F., Naik, V., Stevenson, D. S., Tilmes, S., Voulgarakis, A., Wild, O., Bergmann, D., Cameron-Smith, P., Cionni, I., Collins, W. J., Dalsøren, S. B., Doherty, R. M., Eyring, V., Faluvegi, G., Horowitz, L. W., Josse, B., Lee, Y. H., MacKenzie, I. A., Nagashima, T., Plummer, D. A., Righi, M., Rumbold, S. T., Skeie, R. B., Shindell, D. T., Strode, S. A., Sudo, K., Szopa, S., and Zeng, G.: Pre-industrial to end 21st century projections of tropospheric ozone from the Atmospheric Chemistry and Climate Model Intercomparison Project (ACCMIP), Atmos. Chem. Phys., 13, 2063–2090, doi:10.5194/acp-13-2063-2013, 2013.

Zhang, L., Jacob, D. J., Downey, N. V., Wood, D. A., Blewitt, D., Carouge, C. C., van Donkelaar, A., Jones, D. B. A., Murray, L. T., and Wang, Y.: Improved estimate of the policy-relevant background ozone in the United States using the GEOS-Chem global model with 1/2° × 2/3° horizontal resolution over North America, Atmos. Environ., 45, 6769–6776, doi:10.1016/j.atmosenv.2011.07.054, 2011.





ACPD
13, 11315–11355, 2013



**Table 1.** Mapping table between CAM-Chem and CMAQ.

| CAM-Chem species | Species Name | CMAQ species |
|---|---|---|
| Gas Species | | |
| $O_3$ | Ozone | $O_3$ |
| NO | Nitric oxide | NO |
| $NO_2$ | Nitrogen dioxide | $NO_2$ |
| $NO_3$ | Nitrate radical | $NO_3$ |
| $HNO_3$ | Nitric Acid | $HNO_3$ |
| $HO_2NO_2$ | peroxynitric acid | PNA |
| $N_2O_5$ | Dinitrogen pentoxide | $N_2O_5$ |
| OH | Hydroxyl radical | OH |
| $HO_2$ | Hydroperoxyl radical | $HO_2$ |
| $H_2O_2$ | Hydrogen Peroxide | $H_2O_2$ |
| CO | Carbon monoxide | CO |
| $CH_3OOH$ | Methyl hydroperoxide | MEPX |
| $CH_2O$ | Formaldehyde | FORM |
| $C_2H_4$ | Ethene | ETH |
| $CH_3CHO$ | Acetaldehyde | ALD2 |
| $C_2O_3$ | Acetylperoxy radical | $C_2O_3$ |
| PAN | Peroxyacetyl nitrate | PAN |
| $CH_3COCHO$ | Methylglyoxal and other aromatic products | MGLY |
| ROOH | Higher organic peroxide | ROOH |
| ONIT | Organic nitrate | NTR |
| ISOP | Isoprene | ISOP |
| PAR | Paraffin carbon bond (C-C) | PAR |
| OLE | Terminal olefin carbon bond (R-C=C) | OLE |
| TOLUENE | Toluene and other monoalkyl aromatics | TOL |
| $SO_2$ | Sulfur dioxide | $SO_2$ |
| $C_{10}H_{16}$ | Terpene | TERP |
| $NH_3$ | Ammonia | $NH_3$ |
| $CH_4$ | Methane | $CH_4$ |
| $XO_2$ | NO to $NO_2$ conversion from alkylperoxy ($RO_2$) radical | $XO_2$ |
| $XO_2N$ | NO to organic nitrate conversion from alkylperoxy ($RO_2$) radical | $XO_2N$ |
| ROR | Secondary alkoxy radical | ROR |
| $CL_2$ | Chlorine gas | $CL_2$ |
| HOCL | Hypochlorous acid | HOCL |
| HCL | Hydrogen chloride | HCL |
| Particulate Matters | | |
| $SO_4$ | Sulfate | $ASO_4J$ |
| $NH_4NO_3$ | Ammonium nitrate | ANH4J+ANO3J |
| CB1+CB2 | black carbon, hydrophobic + hydrophillic | AECJ |
| $OC_1 + OC_2$ | organic carbon, hydrophobic + hydrophillic | APOCJ |
| SSLT1+SSLT2 | sea salt, 0.1–0.5 mum, 0.5–1.5 mum | ANAJ/ACLJ |
| SSLT3+SSLT4 | sea salt, 1.–5 mum,–10 ì | ANAK/ACLK |





ACPD
13, 11315–11355, 2013



**Table 2.** Projection factor for anthropogenic emissions in US.

| | Present climate | | | | 2005(Tg) | RCP 4.5 | | | RCP 8.5 | | |
|---|---|---|---|---|---|---|---|---|---|---|---|
| | 2001 | 2002 | 2003 | 2004 | | 2057 | 2058 | 2059 | 2057 | 2058 | 2059 |
| CO | 1.142 | 1.194 | 1.129 | 1.065 | 93.030 | 0.272 | 0.268 | 0.264 | 0.246 | 0.243 | 0.240 |
| $NO_x$ | 1.139 | 1.117 | 1.078 | 1.039 | 18.914 | 0.342 | 0.338 | 0.334 | 0.493 | 0.487 | 0.482 |
| $PM_{10}$ | 1.121 | 1.008 | 1.006 | 1.003 | 21.149 | 0.552 | 0.552 | 0.551 | 0.542 | 0.540 | 0.538 |
| $PM_{2.5}$ | 1.282 | 1.022 | 1.015 | 1.007 | 5.456 | 0.761 | 0.754 | 0.747 | 0.422 | 0.417 | 0.413 |
| SO2 | 1.092 | 1.012 | 1.008 | 1.004 | 14.594 | 0.169 | 0.166 | 0.163 | 0.148 | 0.137 | 0.126 |
| NMVOC | 0.929 | 1.149 | 1.112 | 1.074 | 18.421 | 0.632 | 0.630 | 0.628 | 0.314 | 0.310 | 0.306 |
| $NH_3$ | 0.904 | 1.012 | 1.008 | 1.004 | 4.085 | 1.254 | 1.253 | 1.252 | 1.536 | 1.544 | 1.551 |
| $CH_4$ | 1.202 | 1.187 | 1.172 | 1.156 | 32.180 | 0.893 | 0.888 | 0.883 | 1.612 | 1.626 | 1.640 |
| BC | 1.007 | 1.005 | 1.004 | 1.002 | 0.394 | 0.723 | 0.716 | 0.709 | 0.264 | 0.262 | 0.260 |
| OC | 1.145 | 1.109 | 1.073 | 1.036 | 1.141 | 1.060 | 1.051 | 1.042 | 0.609 | 0.606 | 0.604 |





ACPD
13, 11315–11355, 2013



**Table 3.** Statistical evaluations of CMAQ outputs in comparison to AQS.

| | CO | $NO_2$ | $O_3$-40[1] | $O_3$-60[2] |
|---|---|---|---|---|
| MFB | −29 ± 2 | −9 ± 3 | −5 ± 1 | −21 ± 1 |
| MFE | 83 ± 3 | 80 ± 1 | 27 ± 1 | 28 ± 1 |
| NMB | −41 ± 2 | −4 ± 3 | −1 ± 1 | −17 ± 1 |
| NME | 63 ± 1 | 71 ± 2 | 25 ± 1 | 24 ± 1 |
| MNB | – | – | 1 ± 1 | −16 ± 1 |
| MNE | – | – | 26 ± 1 | 23 ± 1 |
| Benchmark | | | 15/35 | 15/35 |

[1] A cutoff value of 40 ppbv is set.
[2] A cutoff value of 60 ppbv is set.





ACPD
13, 11315–11355, 2013



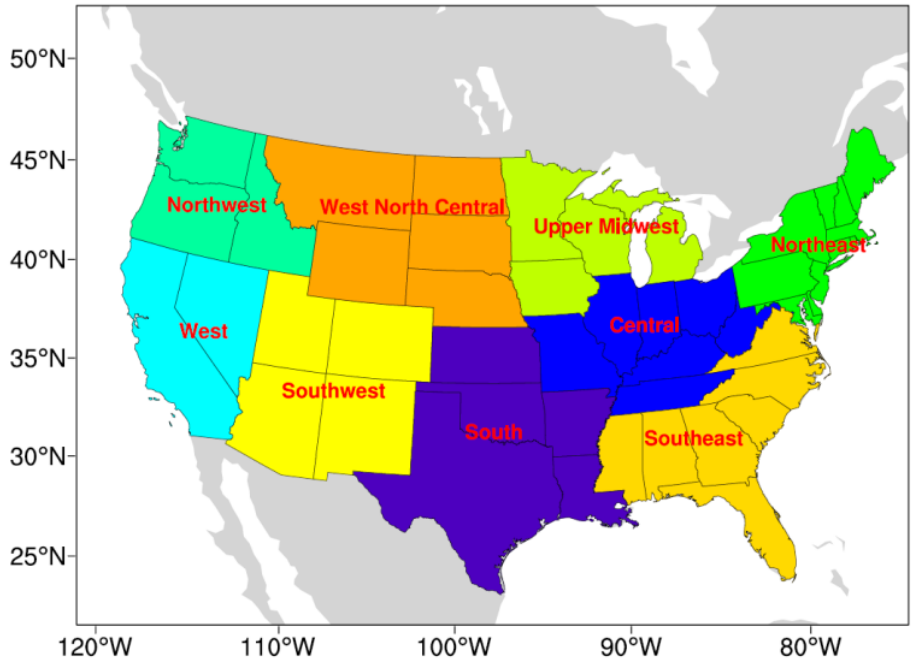


**Fig. 1.** 12 km by 12 km simulation domain with nine climate regions in US.





ACPD
13, 11315–11355, 2013



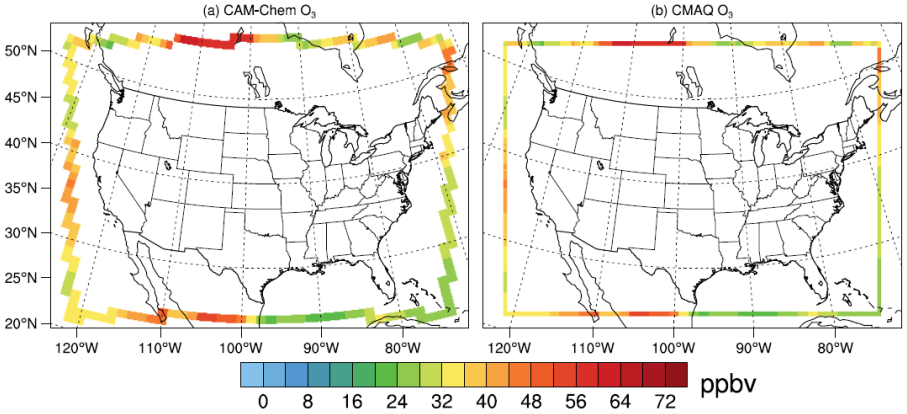


**Fig. 2.** Boundary comparisons between CAM-Chem and CMAQ for $O_3$ concentrations on 1 July 2001, for example.





ACPD
13, 11315–11355, 2013

The impact of emissions and climate change on ozone

Y. Gao et al.



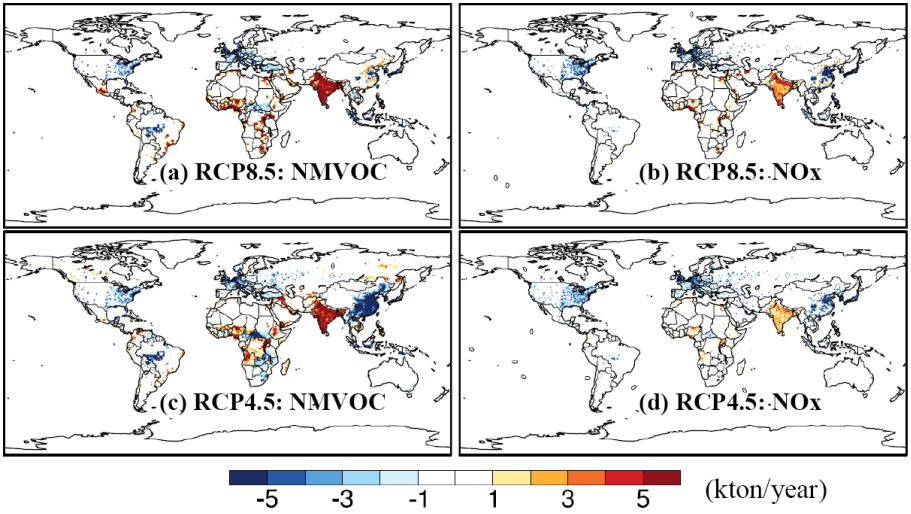


**Fig. 3.** Differences of NMVOCs and $NO_x$ between 2005 and 2060 (2060–2005) for NMVOCs and $NO_x$ in RCP 4.5 and RCP 8.5.





ACPD
13, 11315–11355, 2013



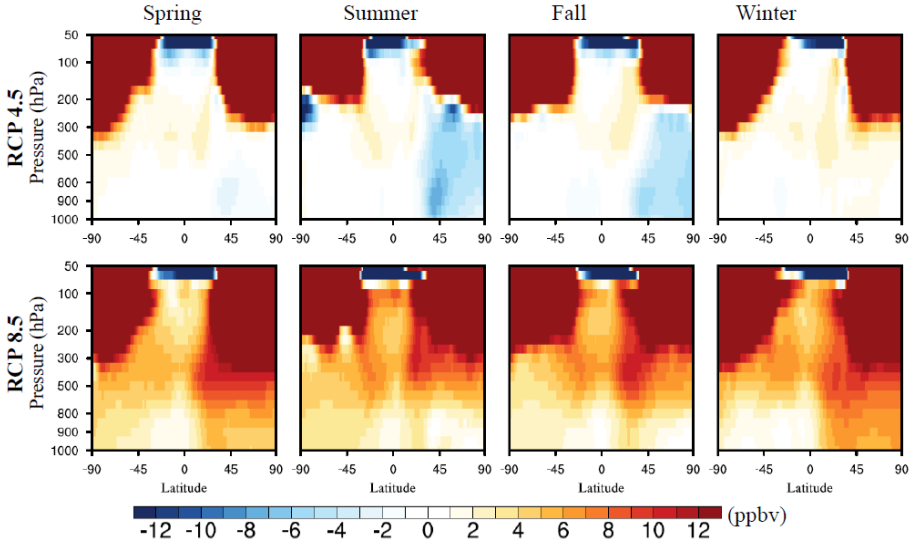


**Fig. 4.** Zonal mean vertical ozone changes from CAM-Chem under future climate (2050–2059 minus 2001–2010) for RCP 4.5 (top panel) and RCP 8.5 (bottom panel). The season definitions are based on the Northern Hemisphere.





ACPD
13, 11315–11355, 2013



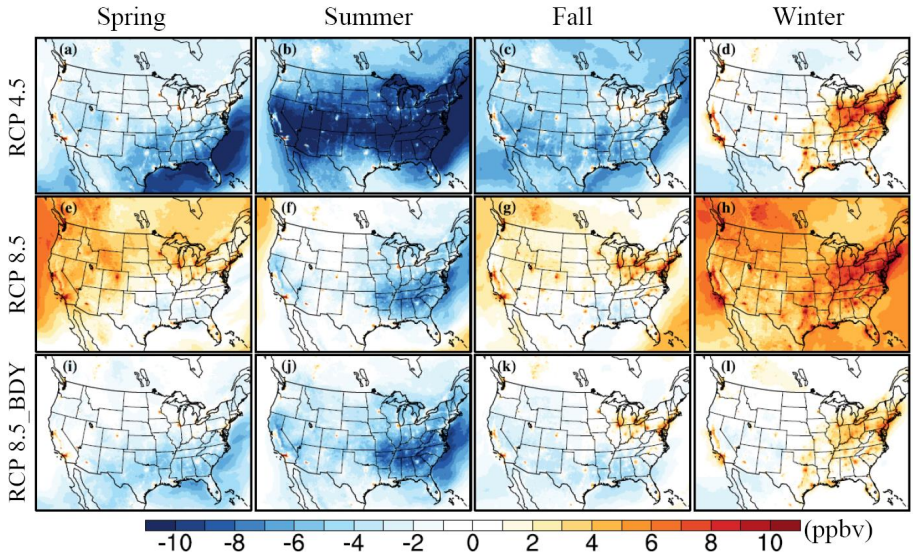


**Fig. 5.** Seasonal mean ozone changes from CMAQ outputs under future climate (2057–2059 minus 2001–2004) for RCP 4.5 **(a–d)**, RCP 8.5 **(e–h)**, RCP 8.5 with present (2001–2004) boundary conditions **(i–l)**.





ACPD
13, 11315–11355, 2013



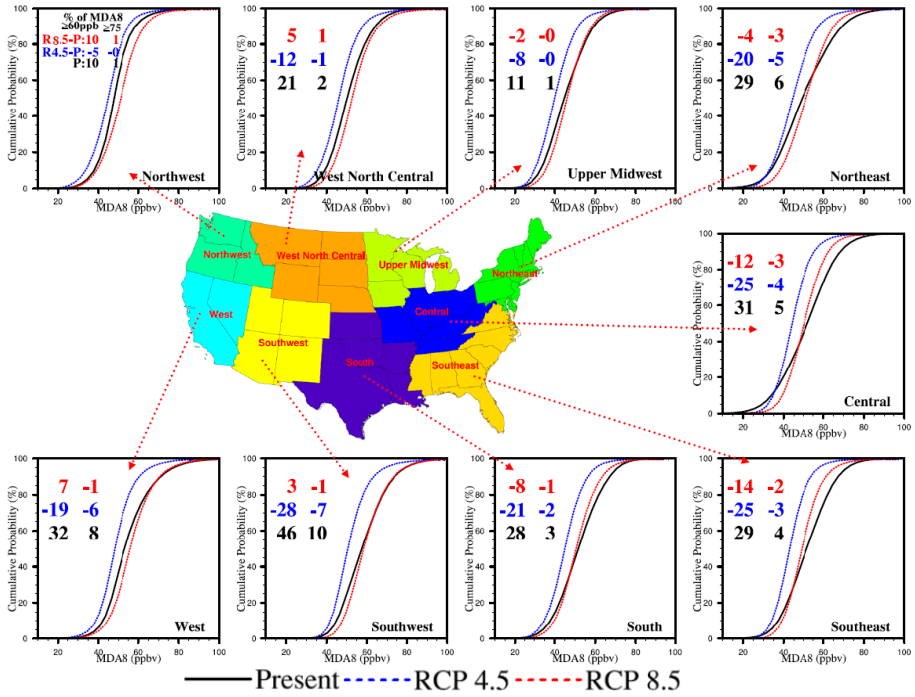


**Fig. 6.** Cumulative distributions of MDA8 ozone from CMAQ. The black, blue and red colors represent the distributions of MDA8 at present climate (2001–2004), RCP 4.5 (2057–2059) and RCP 8.5 (2057–2059), respectively. There are two columns of numbers: the numbers on the left show the percentage of MDA8 ozone exceeding 60 ppbv at present, the percentage change in RCP 4.5 (blue) and RCP 8.5 (red) compared with present; the numbers on the right are similar as left but for MDA8 ozone exceeding 75 ppbv.





ACPD
13, 11315–11355, 2013



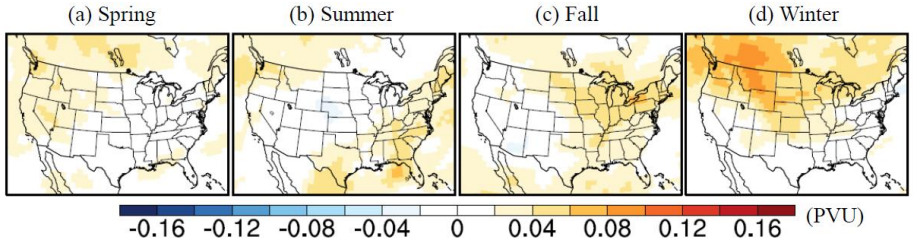


**Fig. 7.** Seasonal mean potential vorticity (PV) changes from CAM-Chem outputs under future climate (2050–2059 minus 2001–2010) for RCP 8.5.





ACPD
13, 11315–11355, 2013



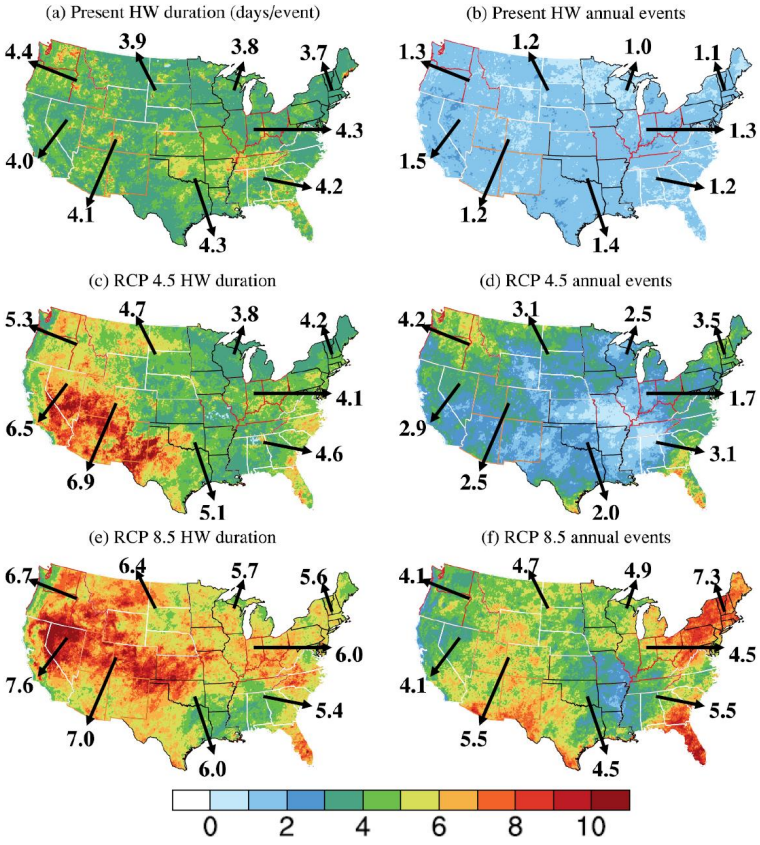


**Fig. 8.** The heat wave duration and frequency. The state boundary was labeled with different colors to distinguish different regions as shown in Fig. 1. The numbers next to the arrows represent the regional mean heat wave duration or frequency.





ACPD
13, 11315–11355, 2013

The impact of emissions and climate change on ozone

Y. Gao et al.



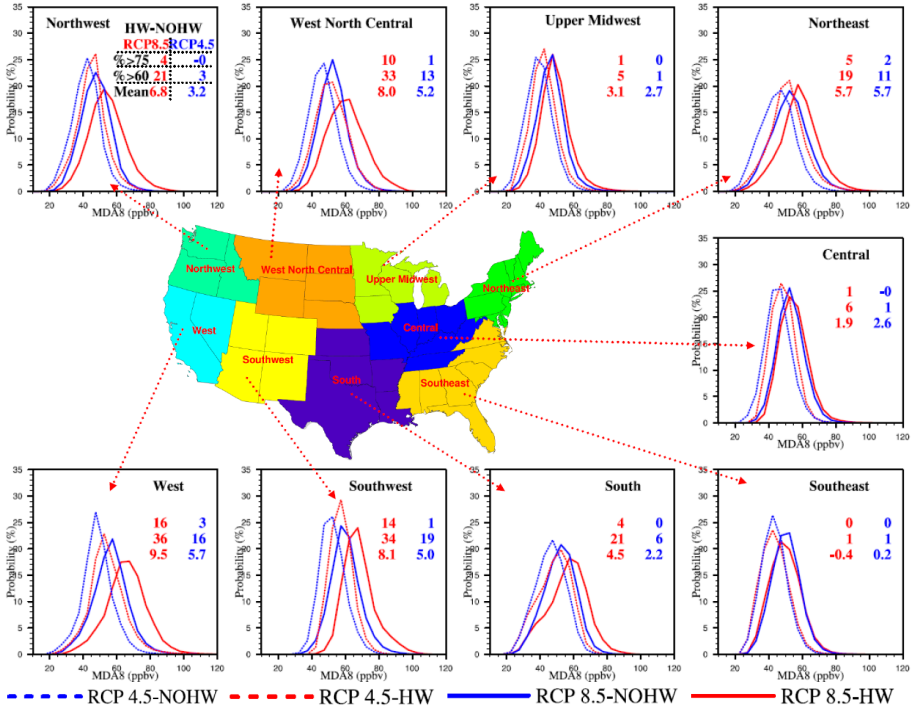


**Fig. 9.** Distributions of MDA8 during the heat wave period and other period (no heat wave) for RCP 4.5 and RCP 8.5 from June to October. There are two columns of numbers, and they represent the differences of mean MDA8 ozone, percentage greater than 75 ppbv and 60 ppbv between heat wave period (referred to as HW) and other period (referred to as NOHW) for RCP 4.5 and RCP 8.5.





ACPD
13, 11315–11355, 2013

The impact of emissions and climate change on ozone

Y. Gao et al.